Article

Taguchi L$_9$ (3^4) Orthogonal Array Design for Photocatalytic Degradation of Methylene Blue Dye by Green ZnO Particles Biosynthesized by *Chrysanthemum* spp. Flower Extract

Thuan Van Tran [1] , **Mabkhoot Alsaiari** [2,3] , **Farid A. Harraz** [2] , **Walid Nabgan** [4] , **Dinh Tien Dung Nguyen** [5] **and Chi Van Nguyen** [6,*]

1 Institute of Applied Technology and Sustainable Development, Nguyen Tat Thanh University, 298-300A Nguyen Tat Thanh, District 4, Ho Chi Minh City 755414, Vietnam; tranuv@gmail.com
2 Promising Centre for Sensors and Electronic Devices (PCSED), Advanced Materials and Nano Research Centre, Najran University, Najran 11001, Saudi Arabia; mabkhoot.alsaiari@gmail.com (M.A.); faharraz@nu.edu.sa (F.A.H.)
3 Empty Quarter Research Unit, Department of Chemistry, College of Science and Art in Sharurah, Najran University, Sharurah 68342, Saudi Arabia
4 Departament d'Enginyeria Química, Universitat Rovira i Virgili, Av. Països Catalans 26, 43007 Tarragona, Spain; wnabgan@gmail.com
5 Institute of Applied Materials Science, Vietnam Academy of Science and Technology, Ho Chi Minh City 700000, Vietnam; tiendungnguyen2201@gmail.com
6 Faculty of Applied Technology, School of Engineering and Technology, Van Lang University, 69/68 Dang Thuy Tram, Binh Thanh District, Ho Chi Minh City 700000, Vietnam
* Correspondence: chi.nv@vlu.edu.vn

Abstract: The pollution of synthetic dyes in wastewater exerts many negative impacts on the environment and human health. There is an increasing demand for the degradation of dyes, with an emphasis on photocatalysis. Here, we investigated the bio-mediated synthesis of ZnO using *Chrysanthemum* spp. flower extract and its utilization for the removal of methylene blue dye under sunlight irradiation. The bandgap energy of green ZnO nanoparticles was determined to be 3.0. The Taguchi L$_9$ (3^4) orthogonal array design was applied to optimize the photocatalytic degradation of methylene blue dye by green ZnO particles. Four parameters, including the initial concentration (10–50 mg/L), ZnO dosage (0.33–1.0 mg), contact time (30–120 min), and pH (4–10) of the solution, were surveyed based on the Taguchi design. We found that the test result (99.0%) at 10 mg/L was almost equivalent to the predicted value (99.5%) of degradation efficiency. The reaction mechanisms shed light on the major role of reactive oxygen species ($^\bullet O_2^-$, $^\bullet OH$). More importantly, the green ZnO particles could be reused for at least five cycles and demonstrated high stability.

Keywords: ZnO particles; photocatalytic degradation; *Chrysanthemum* spp. flower extract; Taguchi design; wastewater treatment

1. Introduction

The growth of the industrial sector has resulted in the discharge of large amounts of toxic waste into the environment, representing a globally critical problem [1]. For example, the synthetic dyes used for printing and textile and paper production are among the most heavily consumed organic compounds [2]. Over the past few decades, the considerable amount of synthetic dye in wastewater has caused many negative impacts on the environment and human health [3]. As a typical dye, methylene blue has shown toxic effects in humans, including carcinogenicity, hypertension, and skin irritation [4]. Some works have also reported that the presence of this dye in water significantly reduces the intensity of light, decreasing the photosynthesis performance of aquatic microorganisms [5]. It has been noted that methylene blue dye contributes to unbalancing aquatic ecosystems

and lessening the quality of water sources [6]. As a result, the treatment of dye contaminants is worthy of consideration [7].

Zinc oxide (ZnO) nanoparticles possess many crystalline structures such as wurtzite, zinc blende, and rocksalt, with a wide range of bandgaps (3.1–3.8 eV) [8]. ZnO nanomaterials have demonstrated their promise in antibacterial, photocatalysis, adsorption, semiconductor, biosensor, nanofertilizer, and nanopesticide applications [9]. Many works have reported the excellent performance of ZnO particles in the photocatalytic degradation of pollutants [10]. For example, Ameen et al. [11] reported a high degradation efficiency of 93% against methylene blue dye using green ZnO synthesized from the *Acremonium potronii* fungal species. Using the hydrothermal method, Zaidi et al. [12] obtained ZnO nanospheres with a bandgap of 3.22 eV. The photocatalytic reaction of Bismarck brown dye reached a pseudo-first-order rate constant of 0.018 min^{-1} and a degradation efficiency of 94%. Chen et al. [13] successfully synthesized ZnO photocatalysts by the sol–gel method at a calcination temperature of 400 °C. They reported that 99.7% of the methyl orange was removed by the ZnO particles. Davari et al. [14] modified ZnO with 6 mol.% Fe_2O_3, achieving a high surface area of 291.35 m^2/g and a bandgap energy of 3.38 eV. Using a response surface methodology, they optimized the photocatalytic performance of ZnO/Fe_2O_3 (99.0%) in the presence of a H_2O_2 oxidant. Because of their high photocatalytic activity, the synthesis of ZnO particles has recently been paid much attention.

There are a number of methods for synthesizing ZnO particles, e.g., chemical coprecipitation and the sol–gel, hydrothermal, and organometallic methods [15]. However, such approaches have many disadvantages relating to the use of toxic chemicals during the synthesis of ZnO particles. To minimize the harmful effects of chemicals, green synthesis with an emphasis on plant extracts has been widely used in previous works. Nguyen et al. [16] reported that natural compounds such as polyphenols, quercetin, kaempferol, reducing sugars, gallic acid, and flavonoids extracted from plants or plant tissues can aid in the reduction and stabilization of ZnO. Moreover, green ZnO showed better antimicrobial activity and less toxicity than chemically synthesized ZnO particles [17–19]. Indeed, Nguyen et al. [20] demonstrated the multiple functions of green ZnO particles as excellent agrichemical adsorbent photocatalysts against methylene blue dye. Asha et al. [21] showed the biological performance of *Piper-longum*-mediated ZnO nanoparticles with a hexagonal wurtzite structure in terms of their antibacterial activity against *S. aureus* and *E. coli*. In a recent study, Bhattacharjee et al. [22] overviewed the potential of biologically synthesized ZnO nanoparticles for photocatalytic applications. The authors also discussed various optimization methods, such as univariate, multivariate, and linear regression methods, for the removal of pollutants. Among these techniques, chemometrics using mathematical and statistical methods is the most powerful approach to obtain the optimum results. Therefore, the importance of optimization methods should be noted.

The Taguchi orthogonal array (L$_9$) is considered one of the most effective approaches for multivariate optimization to obtain target responses [23]. This method is primarily used to design an experimental space with appropriate variables for a small number of trials [24]. The Taguchi method also allows one to evaluate the contribution and effect of each operating factor in the experiment [25]. The prediction of results when applying the Taguchi orthogonal array can be conducted through a confirmation test. The coefficient of determination and probability value are calculated to decide whether the model is reliable. Herein, the Taguchi orthogonal array was applied to optimize the photocatalytic degradation efficiency of methylene blue using green ZnO particles. We designed an experimental space of four factors including dye concentration (A), dose (B), time (C), and pH (D), with an array (3^4) of nine experimental runs. The photocatalytic experiments were independently conducted in batch mode. The green ZnO particles were produced using the flower extract of *Chrysanthemum* spp. and characterized by several physicochemical techniques. The material was recycled many times and structurally analyzed to assess its stability. To the best of our knowledge, the green synthesis and characterization of green ZnO particles using *Chrysanthemum* spp. flower extract has not been investigated previously.

Furthermore, the application of the Taguchi orthogonal array for the optimization of methylene blue degradation using green ZnO has not been addressed in any publication.

2. Materials and Methods

2.1. Preparation of Chrysanthemum spp. Flower Extract

The fresh flowers of *Chrysanthemum* spp. plants were collected from the market, washed with distilled H_2O to remove dirt, and then dried in an oven. The dried flowers (2.0 g) were immersed in 100 mL of distilled H_2O and placed into an ultrasound bath (60 W). The ultrasound-assisted extraction of *Chrysanthemum* spp. flowers was conducted at 60 °C for 60 min. To remove the aqueous extract, the mixture was centrifuged at 6000 rpm for 10 min. The extract solution was stored in a refrigerator at 10 °C.

2.2. Preparation of ZnO Particles Using Chrysanthemum spp. Flower Extract

The synthesis of ZnO particles using the *Chrysanthemum* spp. flower extract was conducted without the addition of alkaline or other chemicals to obtain completely green targets, following a recent publication [20]. Accordingly, 14.0 g of $Zn(NO_3)_2 \cdot 6H_2O$ (98% purity) was added to 350 mL of *Chrysanthemum* spp. flower extract. The mixture was completely dissolved and placed in an ultrasound bath (60 W) at 60 °C for 2 h. The liquid was dried at 120 °C to obtain a soft paste. The formation of green ZnO particles was achieved by calcinating the paste sample in a muffle furnace at 600 °C for 60 min. Ultimately, green ZnO particles were collected and stored for subsequent characterization and photocatalytic experiments.

2.3. Characterization of Green ZnO Particles

The surface morphology of the green ZnO particles was investigated by scanning electron microscopy (SEM) using a multi-purpose JSM-6510 scanning electron microscope (JEOL/EO, Tokyo, Japan) equipped with energy dispersive X-ray spectroscopy (EDX) capabilities. The crystal phase structure of the green ZnO particles was examined by X-ray diffraction (XRD) on a D8 Advance Bruker powder diffractometer (Hitachi Inc., Krefeld, Germany) with Cu–Kα radiation (λ = 1.5406 Å) beams as excitation sources. The Fourier-transform infrared spectroscopy (FT-IR) spectra were recorded on a Nicolet 6700 spectrophotometer (Thermo Fischer Scientific Inc., Waltham, MA, USA). An ultraviolet (UV–Vis) spectrophotometer (Shimadzu, Kyoto, Japan) was used to determine the concentration of methylene blue dye at a wavelength of 665 nm.

2.4. Photocatalytic Activities of Green ZnO Particles

Photocatalytic batch experiments involving the green ZnO particles were conducted under solar illumination between 11:00 and 14:30, when ultraviolet irradiation has the strongest intensity. The experimental design was based on the Taguchi orthogonal array to elucidate the interaction between the operating factors. An experimental space comprising 4 factors, including the dye concentration (A), dosage (B), contact time (C), and pH (D), with an array (3^4) of 9 experimental runs was established, as shown in Table 1. In detail, the ZnO catalyst at a dosage of 0.33–1.0 g/L was added to 30 mL of methylene blue dye at a concentration of 10–50 mg/L and pH 4–10. The mixture was agitated for 60 min under dark conditions so that an adsorption equilibrium was established. The experimental samples were exposed to sunlight irradiation for 30–120 min. An aliquot of each sample was taken to determine the concentration of methylene blue after the photocatalytic process.

Table 1. List of the four operating factors and their levels.

Factor	Unit	Code	Level 1	Level 2	Level 3
Initial dye concentration	mg/L	A	10	30	50
ZnO dosage	g/L	B	0.33	0.67	1.0
Contact time	min	C	30	60	120
pH	-	D	4	7	10

To measure the photocatalytic efficiency of the green ZnO particles, the degradation efficiency *RE* (%) was defined by Equation (1).

$$RE\ (\%) = \frac{C_o - C_e}{C_o} \times 100 \tag{1}$$

where C_o, and C_e are the concentrations (mg/L) of methylene blue dye before and after the photocatalytic treatment.

3. Results and Discussion

3.1. Characterization of Green ZnO Particles

In this work, optical analysis was performed to confirm the formation of green ZnO particles synthesized using *Chrysanthemum* spp. flower extract. Figure 1a shows the UV–visible absorption spectra of Zn^{2+}, *Chrysanthemum* spp. flower extract, and ZnO particles. Accordingly, a maximum absorption peak at 324 nm was observed for the ZnO particles. Figure 1b also indicates a color change from light yellow to brown when Zn^{2+} was added to the *Chrysanthemum* spp. flower extract under ultrasound irradiation at 60 °C. This phenomenon may be explained by the fact that *Chrysanthemum* spp. flower extract contains a number of natural compounds such as folic acid, polyphenols, niacin, quercetin, reducing sugars, and flavonoids [26]. These substrates have functional groups that can chelate with Zn^{2+} ions to generate Zn^{2+}–natural compound complexes. Under heating and microwave irradiation conditions, the complexes can be converted into ZnO particles. The same maximum absorption value was reported in several recent works that used *C. fistula* and *M. azedarach* [27] and *Cayratia pedata* [28] plant extracts for the bio-mediated synthesis of ZnO particles.
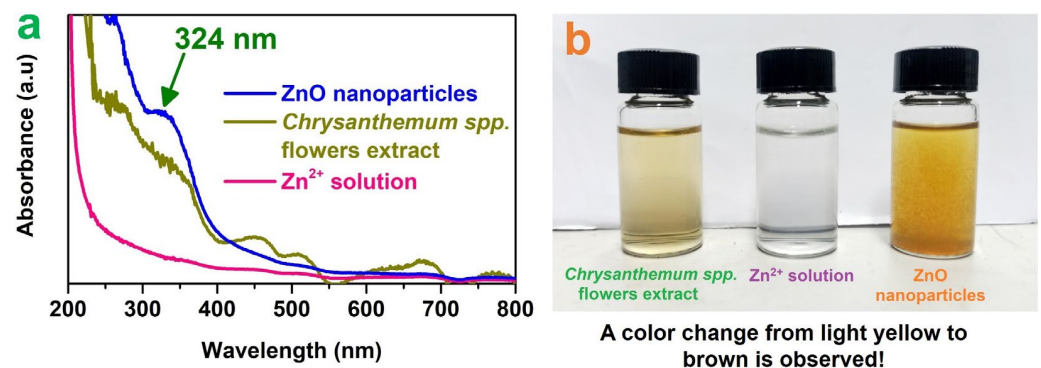

Figure 1. Optical analysis of green ZnO particles synthesized using *Chrysanthemum* spp. flower extract. (**a**) UV–visible absorption spectra of Zn^{2+}, *Chrysanthemum* spp. flower extract, and ZnO particles; (**b**) a color change from light yellow to brown was observed when Zn^{2+} was added to *Chrysanthemum* spp. flower extract under ultrasound irradiation at 60 °C, indicating the formation of green ZnO particles.

The optical analysis of the green ZnO particles could be better elucidated by UV–visible diffuse reflectance spectroscopy. We observed an absorption edge located between 400 and 420 nm. To determine the bandgap energy of the green ZnO particles, the Tauc equation (Equation (2)) could be used.

$$E_g = \frac{hc}{\lambda} = \frac{1240}{\lambda} \tag{2}$$

where E_g denotes the bandgap (eV) of the ZnO particles, h denotes Planck's constant (6.63×10^{-34} J·s), λ (nm) denotes the maximum absorption wavelength, and c denotes the velocity of light [29]. The Tauc plot of $(\alpha h\nu)^2$ versus $(h\nu)$ was established to calculate the bandgap of the ZnO particles. Figure 2 exhibits a bandgap energy of 3.0 eV for fresh ZnO particles synthesized using *Chrysanthemum* spp. flower extract. This value was well

commensurate with the bandgap energy values of both chemically synthesized and bio-mediated ZnO published in the literature [20,30,31]. Therefore, the green ZnO particles could serve as a photocatalyst under solar light illumination, including both ultraviolet and visible light.
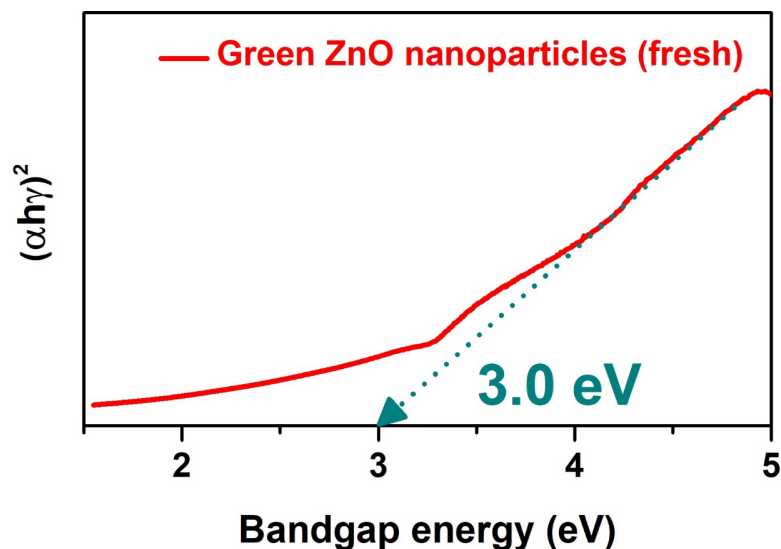

Figure 2. Tauc plot of $(\alpha h\nu)^2$ versus bandgap energy $(h\nu)$ of fresh ZnO particles synthesized using *Chrysanthemum* spp. flower extract.

Herein, the chemical bonding properties of green ZnO particles synthesized using *Chrysanthemum* spp. flower extract were determined using FT-IR spectroscopy (Table 2). According to Figure 3, a range of peaks at 530–715 cm^{-1} was assigned to hexagonal-phase Zn–O bonding, confirming the formation of ZnO particles. The location of these characteristic peaks was in good accordance with previous works [20,27,32]. The existence of primary amines, with N–H stretching vibrations, on the surface of the green ZnO particles could be demonstrated by the typical peak at 860.1 cm^{-1} [33]. Meanwhile, C–O stretching, diagnosed by a peak at 1124 cm^{-1}, was attributable to secondary or tertiary alcohols. Strong C–H bending footprints, belonging to aldehydes or reducing sugars, were observed at 1390 cm^{-1} [33]. While alkene compounds could be identified at 1632 cm^{-1}, there was a narrow peak at 1746 cm^{-1}, ascribed to the C=O stretching of carbonyl groups of esters, δ-lactone, or ketones [34]. The strong absorbance intensity of the peak at 2300 cm^{-1} (C–N/C=N) may have been due to the presence of tertiary amines or imines. At 2385 cm^{-1}, the sharp band of C=C bending may have belonged to aromatic compounds, e.g., quinones, coumarins, tannins, or terpenes (such as carotenoids) [35]. The very typical signals at 2858–2923 cm^{-1} were due to the absorbance of symmetric methylene groups (CH$_2$), aliphatic groups, or aldehydes from natural compounds. We observed N–H vibrations (broad band) at 3450 cm^{-1}, which could have signaled amide groups, primary amines or proteins from alkaloids, or betalains in the *Chrysanthemum* spp. flower extract. Finally, a medium band of O–H vibrations at 3730 cm^{-1} could be assigned to either hydroxyl groups of alcohols, polyphenols, polysaccharides, quercetin, genin, or gallic acid in the *Chrysanthemum* spp. flower extract, or surface-chemisorbed H$_2$O [36]. Several works have reported the same chemical bonds in hexagonal-phase ZnO particles synthesized by bio-based methods using the extracts of various plants, such as *Phlomis* leaves [32], *Cassia fistula* and *Melia azedarach* leaves [27], *Canna indica* flowers [20], and *Myristica fragrans* fruit [37]. Therefore, the surface of the hexagonal-phase green ZnO nanoparticles synthesized using *Chrysanthemum* spp. flower extract contained a variety of functional groups, which were expected to have good photocatalytic activity.

Table 2. Surface chemistry of green ZnO particles synthesized using *Chrysanthemum* spp. flower extract.

No.	Position	Chemical Bonds	Compounds	Reference
1	3730 cm^{-1}	A medium band of O–H vibrations	Hydroxyl groups of alcohols, polyphenols, polysaccharides, quercetin, genin, and gallic acid in *Chrysanthemum* spp. flower extract or surface-chemisorbed H$_2$O.	[36]
2	3450 cm^{-1}	N–H vibrations (broad band)	Amide groups, primary amines or proteins from alkaloids, and betalains in *Chrysanthemum* spp. flower extract.	
3	2858–2923 cm^{-1}	C–H stretching (medium band)	Symmetric methylene groups (CH$_2$), aliphatic groups, or aldehydes from natural compounds	
4	2385 cm^{-1}	C=C bending (sharp band)	Aromatic compounds, e.g., quinones, coumarins, tannins, or terpenes (such as carotenoids).	[35]
5	2300 cm^{-1}	C–N/C=N (very sharp band)	Tertiary amines or imines.	
6	1746 cm^{-1}	C=O stretching (narrow band)	Carbonyl groups of esters, δ-lactone, or ketones.	[34]
7	1632 cm^{-1}	C=C stretching (broad, strong band)	Alkenes.	
8	1390 cm^{-1}	C–H bending (strong band)	Aldehydes or reducing sugars.	[33]
9	1124 cm^{-1}	C–O stretching	Secondary or tertiary alcohols.	
10	860.1 cm^{-1}	N–H stretching vibrations	Amines.	[33]
11	530–715 cm^{-1}	Zn–O	The formation of zinc oxide nanoparticles using *Chrysanthemum* spp. flower extract.	[38]
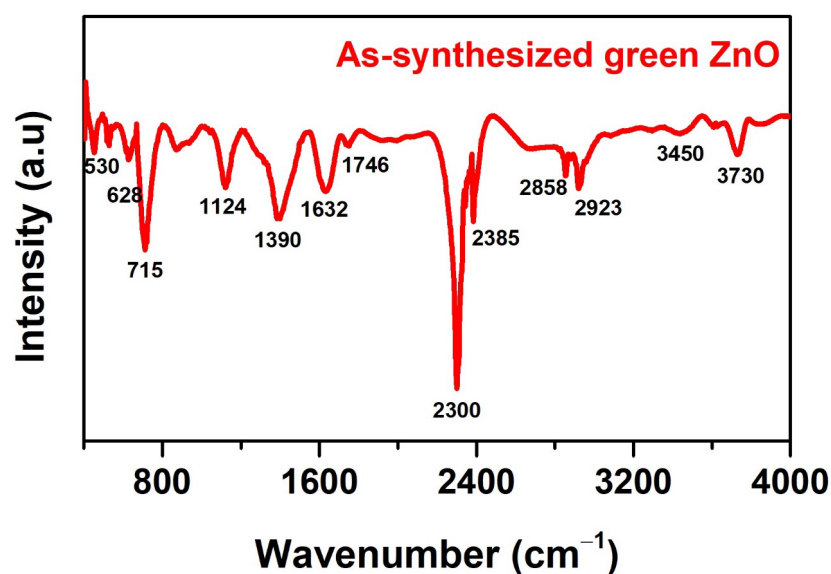
Figure 3. FT-IR spectrum of green ZnO particles synthesized using *Chrysanthemum* spp. flower extract.

To determine the crystalline structure of the green ZnO particles synthesized using *Chrysanthemum* spp. flower extract, the X-ray powder diffraction pattern was observed. As

shown in Figure 4, the green ZnO particles showed a typical XRD pattern with summits (2θ, degrees) located at 31.92° (100), 34.62° (002), 36.52° (101), 47.72° (102), 56.84° (110), 63.18° (103), and 68.36° (112). Moreover, the pattern profile of the as-synthesized ZnO in this work was matched well with the standard reference for ZnO particles (JCPDS #36–1451), as shown in Figure 4. It was also in line with the pattern profile of the hexagonal wurtzite-structured ZnO reported in previous works [20,27,32]. The pattern of the green ZnO particles showed very-high-intensity peaks, and no strange peaks were observed. This indicated that the green ZnO particles synthesized using *Chrysanthemum* spp. flower extract had a high degree of purity. To estimate the average size of the green ZnO particles, Scherer's equation could be used (Equation (3)).

$$D = \frac{K \times \lambda}{\beta \times \cos(\theta)} \tag{3}$$

where K is a constant equal to 0.90, β is the full-width at half-maximum height of the diffraction peaks at Bragg's angle θ, and λ is the wavelength of the X-ray radiation. According to Equation (3), the average size of the green ZnO particles synthesized using *Chrysanthemum* spp. flower extract was estimated to be 30.24 nm. The particle size of the green ZnO particles in this work was in excellent agreement with results from previous studies using extracts such as *Canna indica* flowers (29.85 nm) [20], *Capparis zeylanica* leaves (32 nm) [28], *Solanum nigrum* leaves (29.79 nm) [39], *Costusigneus* leaves (31 nm) [40], and *Uncaria gambir* leaves [41] for the bio-mediated synthesis of ZnO particles.
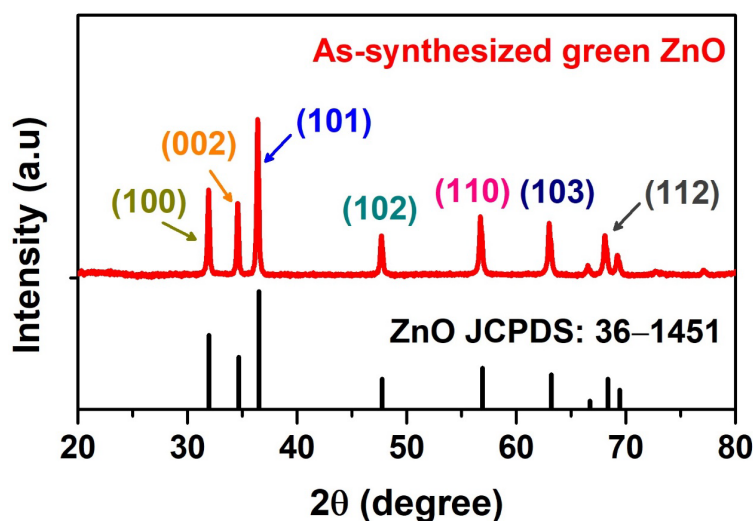

Figure 4. XRD diffraction pattern of green ZnO particles synthesized using *Chrysanthemum* spp. flower extract.

Figure 5 presents the scanning electron microphotographs of the green ZnO particles synthesized using *Chrysanthemum* spp. flower extract. The morphology of the green ZnO particles had a level of agglomeration. Due to the calcination during synthesis, crystals grow under the control of many factors, such as van der Waals forces, polarities, and electrostatic attractions [16]. As a result, ZnO particles can form many defects on their surfaces, which results in a large surface area. This phenomenon is explained by the thermal decomposition of natural compounds in *Chrysanthemum* spp. flower extract, e.g., folic acid, polyphenols, niacin, quercetin, reducing sugars, and flavonoids [26]. The influence of the calcination temperature on the morphology of green ZnO particles was reported by Thi et al. [42]. However, a calcination temperature of 600 °C could be to minimize the self-clustering and agglomeration of green ZnO particles.
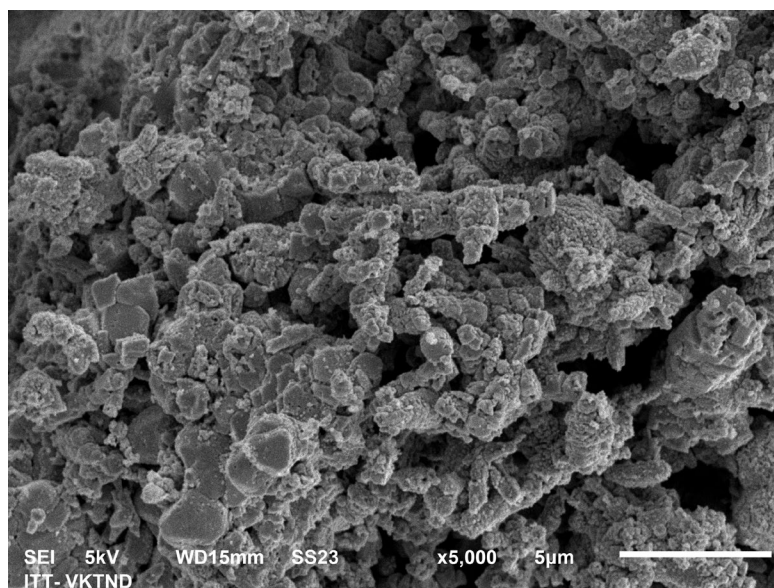
Figure 5. SEM image of green ZnO particles synthesized using *Chrysanthemum* spp. flower extract.

The chemical composition of the green ZnO particles synthesized using *Chrysanthemum* spp. flower extract could be analyzed by energy-dispersive X-ray spectroscopy. According to Figure 6, the ZnO particles contained O and Zn as the main components (>94%) in their structure. Our findings revealed that the ZnO particles had a high degree of purity. A minute amount of other elements such as N (4.23%), Cl (0.29%), P (0.32%), and K (0.96%) was observed in the ZnO nanomaterial. These traces could have come from the *Chrysanthemum* spp flower extract. The calcination of the sample released most of the volatile components, leaving a number of elements in the structure of the ZnO. Several works have reported similar high-purity ZnO particles synthesized using various plant extracts, such as *Hibiscus sabdariffa*, *Cannabis Jatropha*, *Tinosporacordifolia*, *Thymbra spicata*, and *Cinnamomum camphora* [43–46]. As such, ZnO particles could exhibit sufficient photocatalytic activity against organic dyes. To better elucidate this, the green ZnO particles synthesized using *Chrysanthemum* spp. flower extract were further investigated.

Element	Weight %	Sigma %	Atomic %
O	20.19	0.21	48.8
Zn	76.78	0.37	45.4
N	1.53	0.37	4.23
Cl	0.27	0.07	0.29
P	0.26	0.07	0.32
K	0.97	0.11	0.96
Total	100.0		100.0

Figure 6. EDX spectrum and element ratio of green ZnO particles synthesized using *Chrysanthemum* spp. flower extract.

3.2. Taguchi Design and Model Optimization

In this study, the Taguchi design was used to create an experimental space comprising four factors, including dye concentration (A, 10–50 mg/L); ZnO dosage (B, 0.33–1.0 g/L); contact time (C, 30–120 min); and pH (D, 4–10). As shown in Table 3, there were nine experiments in total (entry 1–9) for this design, and the average degradation efficiency value (11.1–96.9%) was 38.66%. To better elucidate the effect of the main parameters, the analysis of variance (ANOVA) conducted based on the Taguchi design (3^4) is presented in Table 4.

Table 3. Taguchi L_9 factor and level combinations for assessing the methylene blue degradation efficiency of green ZnO particles.

No.	A (mg/L)	B (g/L)	C (min)	D (pH)	Removal (%)
1	10	0.33	30	4	18.1
2	10	0.67	60	7	68.8
3	10	1.0	120	10	96.9
4	30	0.33	60	10	35.7
5	30	0.67	120	4	48.9
6	30	1.0	30	7	17.6
7	50	0.33	120	7	35
8	50	0.67	30	10	15.8
9	50	1.0	60	4	11.1

Table 4. ANOVA data for standard average.

Parameter	DF [a]	SSS [b]	SEC [c]	Coefficient	*p* Value [d]
A—Initial concentration (mg/L)	1	2476.6	0.193	−1.016	0.006 [e]
B—Adsorbent dosage (g/L)	1	225.7	0.386	0.613	0.187 [f]
C—Contact time (min)	1	2692.0	0.084	0.462	0.005 [e]
D—pH of the solution (−)	1	823.7	1.287	3.906	0.039 [e]
Total	4	6218.0	–	–	0.009 [e]

Notes: [a] Degree of freedom, [b] sequential sums of squares, [c] standard error of the coefficient, [d] probability, [e] significant at $p < 0.05$, [f] not significant at $p > 0.05$.

The *p* value of the regression was found to be 0.009, corresponding to an F value of 17.38. This value was far lower than 0.05, indicating that the regression model was statistically significant. Moreover, the coefficient of determination R^2 and adjusted R^2 were very high at 0.946 and 0.891, respectively. Therefore, the experimental data in this study offered high reliability. The probability values of terms A, B, C, D could be used to clarify whether they were statistically significant. The results revealed that the initial concentration, contact time, and pH were statistically significant at $p < 0.05$, while the ZnO dose was statistically insignificant. From the ANOVA table, a regression equation was established to show the correlation between the variables and responses, as follows (Equation (4)):

$$\text{Degradation efficiency}(\%) = -2.8 - 1.02A + 18.39B + 0.462C + 3.91D \tag{4}$$

To determine the contribution of the parameters, the value of the sequential sums of squares was calculated. The contribution of each parameter was equal to the ratio between the sequential sums of squares of that parameter and the total sequential sums of squares. According to Figure 7, the most important contributor was contact time, and pH was the least important contributor. The contributions were ranked as follows: contact time (rank 1: 43.29%) > initial concentration (rank 2: 39.83%) > pH of the solution (rank 3: 13.25%) > ZnO dosage (rank 4: 3.63%). Importantly, the contact time and initial concentration contributed to 83% of the total main effect. Figure 8a,b show the effect of these parameters on the degradation efficiency; the optimum conditions were obtained at a low concentration, medium dosage, high reaction time, and high pH.
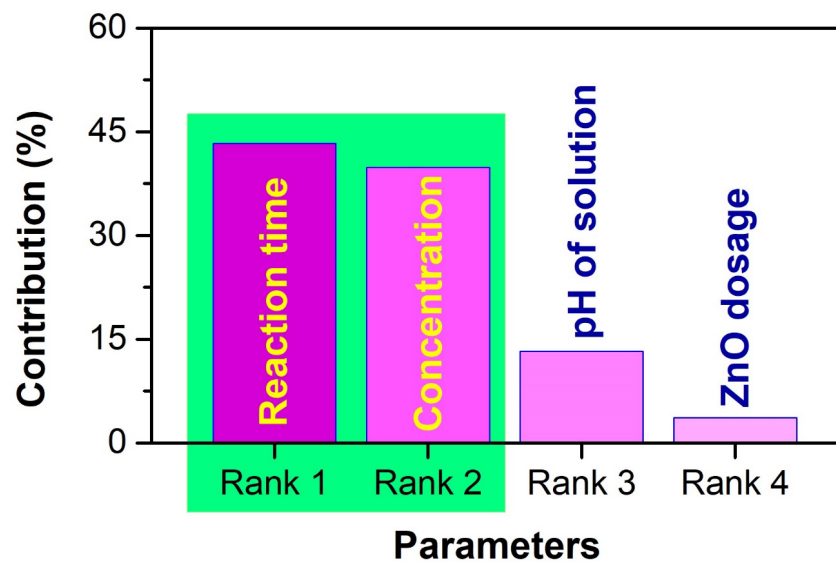
Figure 7. The contribution of each factor to the methylene blue degradation efficiency of green ZnO particles synthesized using *Chrysanthemum* spp. flower extract.
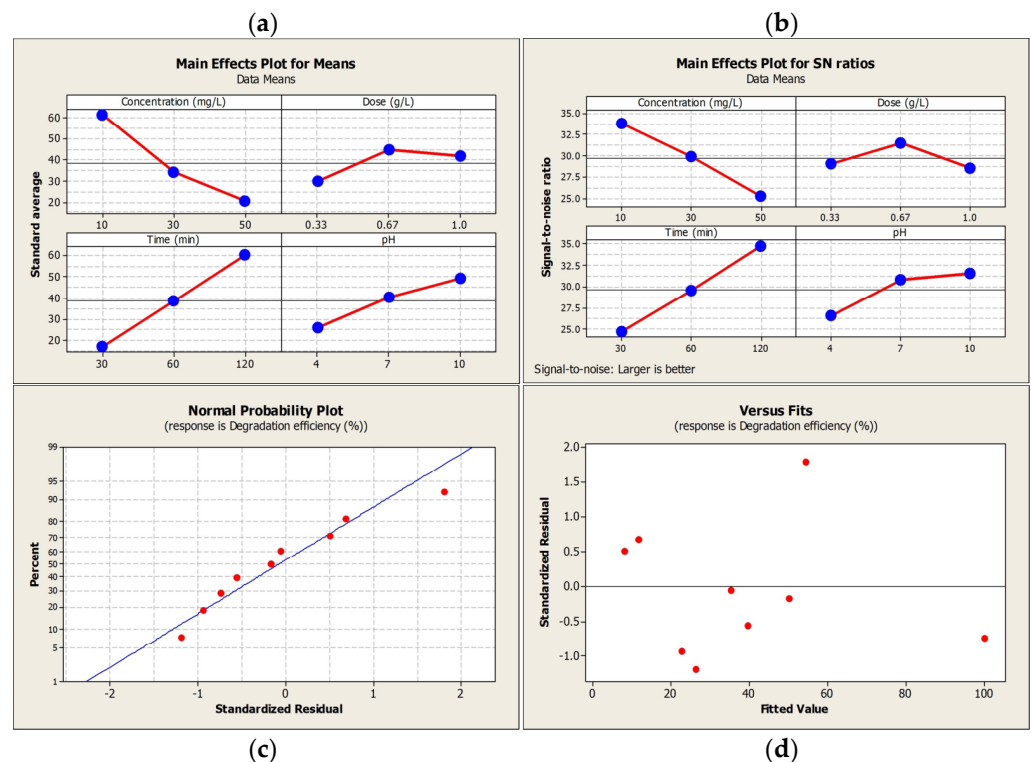

Figure 8. Standard average for means (**a**); signal-to-noise ratio (**b**) for main effects (initial concentration, ZnO dosage, contact time, and pH of the solution); the normal probability plot for standardized residuals (**c**); and the plot of standardized residuals versus fitted values (**d**).

Certain diagnostic plots can be useful for model validation and the assessment of model reliability. Figure 8c provides a visual representation of the data distribution, with red points tending to gather around the blue line. This normal probability plot indicates a high level of compatibility, and there were no abnormal points observed in the dataset. Figure 8d presents the standardized residuals, with all values in the range of −2 to +2. No specific patterns, outliers, or large residuals were observed in the plot. The fitted values were sufficient to ignore the errors caused by the data noise. There was no need to rerun the experiments for adjustment. Therefore, the model was adequate to predict the optimal

results, and the assumptions of the regression model were satisfied with high suitability. Model confirmation was conducted to verify the predictions.

3.3. Model Confirmation

Based on Table 5, the optimal conditions were selected according to the highest signal-to-noise ratio. Accordingly, the optimum value was predicted to be 99.5% when the following conditions were met: initial concentration of 10 mg/L, ZnO dosage of 0.67 g/L, contact time of 120 min, and pH of 10. To verify this prediction, a confirmation test was conducted with the above inputs. We observed that the actual value for the degradation of methylene blue was 99.0%, which was 0.5% lower than the predicated value. This error was minute and acceptable for the model estimation. The Taguchi L_9 (3^4) orthogonal array design was a reliable approach for the optimization of the photocatalytic degradation of methylene blue dye using green ZnO particles.

Table 5. Optimal conditions based on the highest signal-to-noise ratio.

No.	Parameters	Optimized Value	Level	Contribution (%) [a]
1	Initial concentration (mg/L)	10	1	39.83
2	ZnO dosage (g/L)	0.67	2	3.63
3	Contact time (min)	120	3	43.29
4	pH of the solution (-)	10	3	13.25

Note: [a] Predicted value: 99.5%; actual value: 99.0%; relative error: -0.5%.

3.4. Proposed Mechanism for Dye Degradation

To shed light on the photocatalytic mechanism of the green ZnO particles synthesized using Chrysanthemum spp. flower extract, scavenging experiments were conducted. It was important to measure the degradation efficiency of methylene blue by the green ZnO catalyst in the presence of several scavengers, e.g., ascorbic acid, tert-butanol, and ethylenediaminetetraacetic acid. Because the scavengers reacted with active radicals including hydroxyl ($^\bullet$OH), superoxide ($^\bullet O_2^-$), and hole (h^+) radicals, the degradation efficiencies were reduced. We observed that the degradation efficiency of the ZnO catalyst in the presence of scavengers was 41.3% for ascorbic acid, 55.8% for ethylenediaminetetraacetic acid, and 88.0% for tert-butanol. Therefore, the contributions of the radicals to the reaction were ranked as follows: $^\bullet O_2^- > {}^\bullet OH > h^+$. These findings suggested that both $^\bullet O_2^-$ and $^\bullet$OH species played a major role in the degradation of methylene blue dye.

Figure 9 describes the proposed mechanisms of the ZnO catalyst. In detail, the ZnO edges initially absorb photons of solar light to generate electrons (e^-) and holes (h^+). $^\bullet O_2^-$ radical species can be formed via reactions between electrons adsorbed on the conduction band. $^\bullet$OH radical species are generated via a multi-step reaction between holes (h^+) and H_2O/OH^-. Methylene blue also adsorbs photons of solar light to generate radicals. The most important reaction between reactive oxygen species ($^\bullet O_2^-$, $^\bullet$OH) and dye molecules causes the formation of smaller degradation products such as CO_2 and H_2O. The main steps of this plausible photocatalytic reaction are illustrated in Figure 10.

3.5. Recyclability Study

Recyclable catalysts offer many advantages, i.e., reducing the production cost and indirectly minimizing the disposal of pollutants. Therefore, the recyclability of the ZnO catalyst synthesized using *Chrysanthemum* spp. flower extract for the photodegradation of methylene blue dye in water was investigated. The eluent solvents for washing and desorbing the dye molecules from the catalyst were important; hence, ethanol was selected due to its low cost, effectiveness, and safety [47]. After regeneration, the catalyst was subject to a reaction with methylene blue dye under solar light irradiation. The results shown in Figure 11 indicate that the green ZnO could be reused for five sequential cycles. At an MB concentration of 10 mg/L, the first cycle achieved an efficiency of nearly 97%, while the value of the final cycle remained at 60%, revealing the excellent stability and

photocatalytic activity of the green ZnO synthesized using *Chrysanthemum* spp. flower extract. The significant decrease (~37%) in the degradation efficiency of the green ZnO catalyst might be explained by the gradual deactivation of the catalytic ZnO sites after each reuse cycle. Moreover, the washing process in the regeneration of the ZnO might not have been complete, leaving traces of MB dye bound on the surface of the ZnO. As a result, the photocatalytic activity was reduced after each reuse cycle. The same number of reuse cycles (five) for ZnO was reported in previous works [47,48].
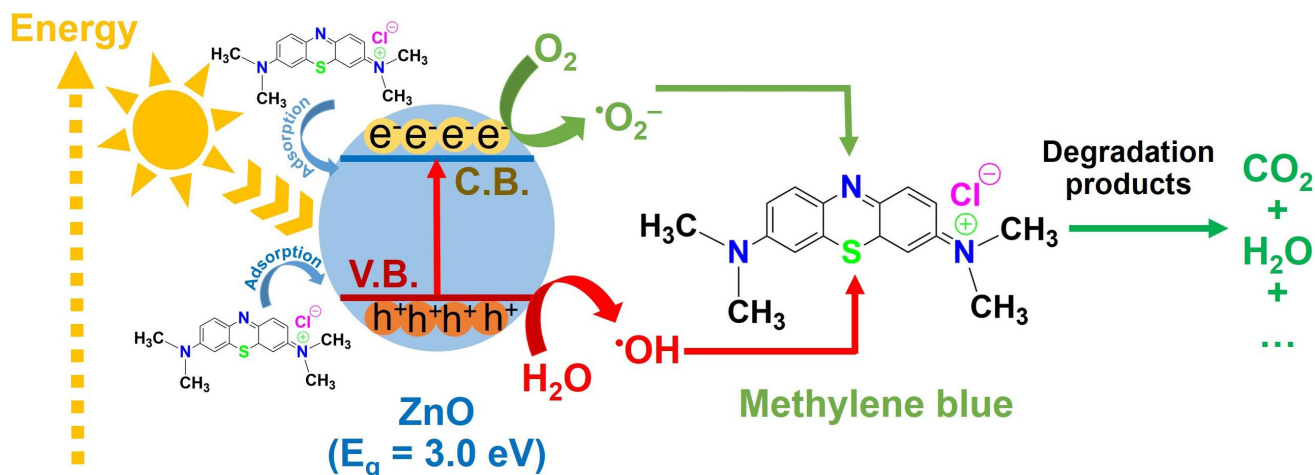

Figure 9. Methylene blue dye degradation mechanism pathways under the catalysis of green ZnO particles synthesized using *Chrysanthemum* spp. flower extract. Abbreviations: conduction band, C.B.; valence band, V.B.; electron, e^-; hole, h^+; reactive oxygen species, $^\bullet O_2^-$ and $^\bullet OH$.

i. $\quad ZnO + h\gamma \longrightarrow e^- + h^+$

ii. $\quad e^- + O_2 \longrightarrow {}^\bullet O_2^-$

iii. $\quad {}^\bullet O_2^- + H^+ \longrightarrow {}^\bullet OOH$

iv. $\quad {}^\bullet OOH + H^+ + e^- \longrightarrow H_2O_2$

v. $\quad H_2O_2 + e^- \longrightarrow {}^\bullet OOH + OH^-$

vi. $\quad h^+ + H_2O \longrightarrow {}^\bullet OH + H^+$

vii. $\quad h^+ + OH^- \longrightarrow {}^\bullet OH$

viii. $\quad MB + visible\ light \longrightarrow [MB]^\bullet$

ix. $\quad {}^\bullet OH + [MB]^\bullet \longrightarrow CO_2 + H_2O + \ldots$

x. $\quad {}^\bullet O_2^- + [MB]^\bullet \longrightarrow CO_2 + H_2O + \ldots$
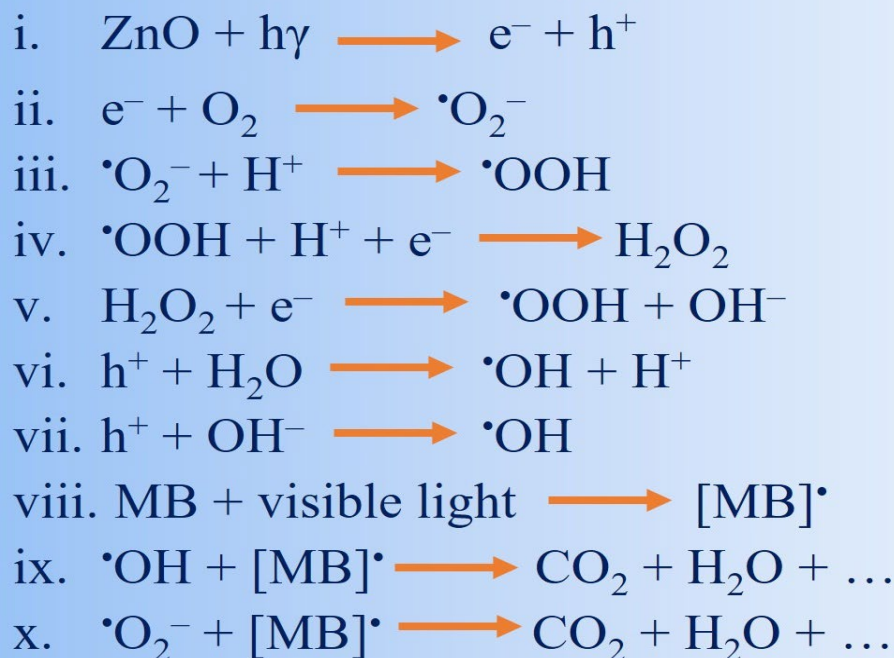
Figure 10. The main steps of the plausible photocatalytic reaction involving the green ZnO catalyst synthesized using *Chrysanthemum* spp. flower extract for the photodegradation of methylene blue dye.
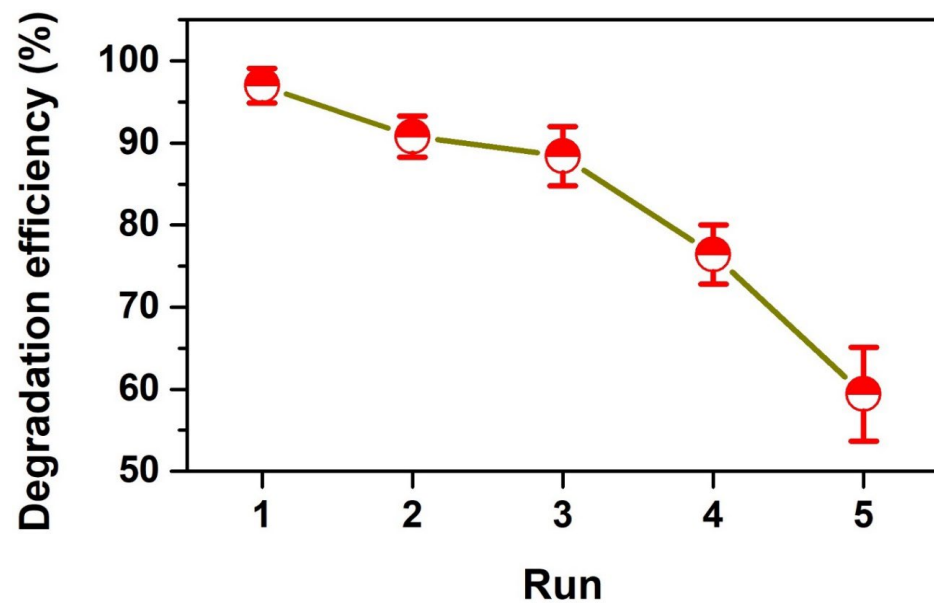
Figure 11. Recyclability of ZnO catalyst synthesized using *Chrysanthemum* spp. flower extract for the photodegradation of methylene blue dye in water.

3.6. Stability Study

The stability of the green ZnO synthesized using *Chrysanthemum* spp. flower extract was assessed using physicochemical analysis. The XRD and FT-IR spectra of the reused and fresh ZnO catalysts after the treatment of methylene blue dye were monitored. As observed from Figure 12, the bandgap energy of the reused ZnO catalyst was 3.0 eV, which was the same as that of the fresh ZnO catalyst. Moreover, Figure 13a shows that some peaks remained for the reused ZnO catalyst. There was also no significant difference in the position of the XRD peaks between the reused and fresh ZnO catalysts. However, the sharp FT-IR peaks at approximately 2300 (C–N/C=N stretching) and 2385 cm^{-1} (C=C bending) were absent. This could be explained by the fact that the crucial functional groups, i.e., tertiary amines, imines, etc., on the surface of the green ZnO particles were significantly reduced. Therefore, a decreasing trend in the photocatalytic activity of the ZnO particles is indicated in Figure 11. Moreover, minor shifts in other peaks can be observed in Figure 13b, indicating that the washing process of the ZnO might not have been complete, leaving trace amounts of MB dye bound on the surface of the ZnO. However, it could be confirmed that the structure of the ZnO catalyst still had high stability under experimental conditions.
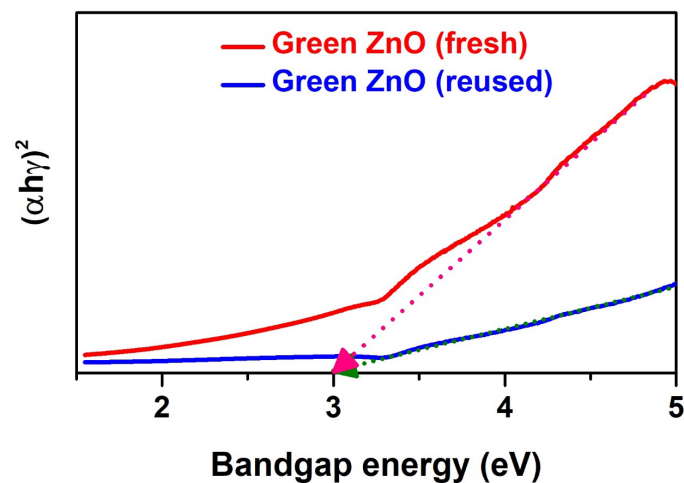

Figure 12. Tauc plot of $(\alpha h\nu)^2$ versus bandgap energy ($h\nu$) of fresh and reused ZnO particles synthesized using *Chrysanthemum* spp. flowers extract.
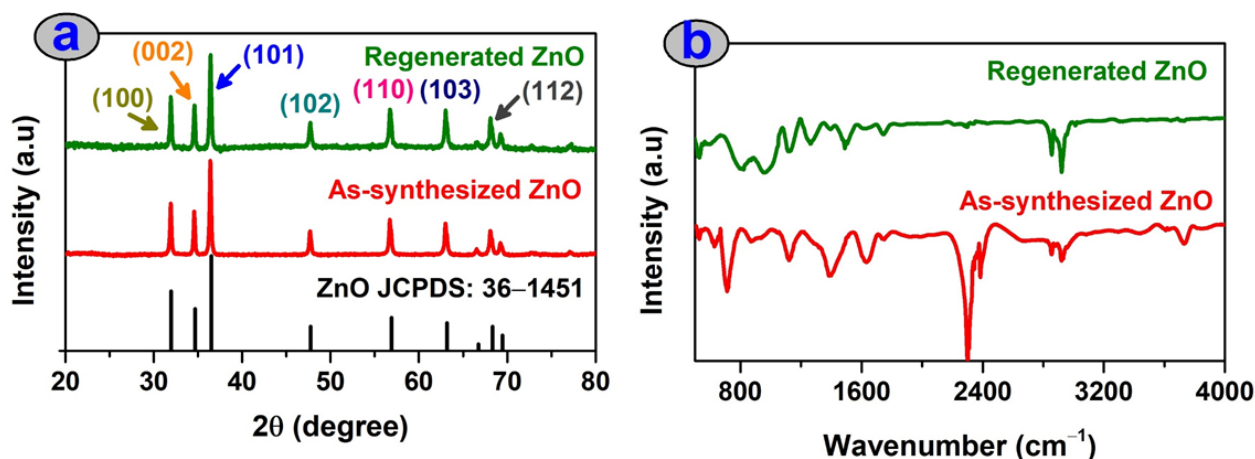
Figure 13. XRD (**a**) and FT-IR (**b**) spectra of reused and fresh ZnO catalysts synthesized using *Chrysanthemum* spp. flower extract for the photodegradation of methylene blue dye in water.

3.7. Comparison Study

To demonstrate the effectiveness of ZnO particles synthesized through various routes, such as bio-mediated and chemical pathways, a comparison study was performed. As shown in Table 6, the photocatalytic methylene blue degradation of ZnO particles synthesized using Chrysanthemum spp. flower extract produced superior results in terms of degradation efficiency and reaction time compared with other ZnO catalysts. Indeed, the green ZnO particles in this study had a degradation efficiency of 99.0%, which was higher than the values for particles synthesized using plant extracts such as Beta vulgaris [49], Myristica fragrans [37], Pithecellobium dulce [50], and Suaeda japonica [51]. We found that this material had a higher degradation efficiency against methylene blue than chemically synthesized ZnO catalysts reported previously [43]. The degradation reaction in this work was performed under solar light irradiation, with a short reaction time of 120 min. Therefore, ZnO particles synthesized using Chrysanthemum spp. flower extract could be an excellent photocatalyst for the degradation of methylene blue dye in aqueous solution in actual wastewaters.

Table 6. Comparison of the photocatalytic degradation of methylene blue dye using ZnO particles synthesized via various pathways.

Method of Synthesis	Light Source	Degradation Efficiency (%)	Catalyst Dose (g/L)	Concentration (mg/L)	Degradation Time (min)	Reference
Bio-mediated (*Chrysanthemum* spp. flowers)	Sunlight	99.0	0.67	10	120	This work
Bio-mediated (jujube fruit)	Sunlight	85.0	1.0	100	300	[30]
Bio-mediated (*Beta vulgaris*)	Ultraviolet light, 370 nm	80.0	0.2	5	150	[49]
Bio-mediated (*Myristica fragrans*)	Ultraviolet light	88.0	0.56	20	140	[37]
Bio-mediated (*Pithecellobium dulce* peel)	Ultraviolet light, 365 nm	63.0	-	320	120	[50]
Bio-mediated (*Justicia spicigera*)	Ultraviolet light, Hg lamp 10 W	81.9	1.0	15	90	[52]
Bio-mediated (*Suaeda japónica*)	Ultraviolet light, 346 nm	54.0	1.0	32	60	[51]
Commercial	Ultraviolet light, Xenon 200 W	66.9	0.5	20	80	[53]

Table 6. *Cont.*

Method of Synthesis	Light Source	Degradation Efficiency (%)	Catalyst Dose (g/L)	Concentration (mg/L)	Degradation Time (min)	Reference
Bio-mediated (*Hibiscus sabdariffa*)	Ultraviolet light, 10 W	97.0	1.0	15	150	[43]
Bio-mediated (*Scutellaria baicalensis*)	Ultraviolet light, 365 nm	98.6	0.1	16	210	[54]
Chemical	Ultraviolet light, 10 W	78.5	1.0	15	120	[43]
Chemical	Sunlight	98.0	0.5	100	30	[55]

4. Conclusions

The Taguchi L_9 (3^4) orthogonal array design was successfully applied to optimize the photocatalytic degradation of methylene blue dye by green ZnO particles synthesized using *Chrysanthemum* spp. flower extract. The reaction time was determined to be the most important contributor (43.29%) to the methylene blue degradation efficiency. The regression model was statistically significant according to the very low *p* value of 0.009. The model had a high coefficient of determination, R^2 = 0.946, which proved the high reliability of the experimental data. The predicted value was 99.5%, which was almost equivalent to the test results at an initial concentration of 10 mg/L, ZnO dosage of 0.67 g/L, contact time of 120 min, and pH of 10. A reaction mechanism was suggested, with the main role being performed by reactive oxygen species ($^\bullet O_2{}^-$, $^\bullet OH$). The green ZnO particles could be reused for at least five cycles and exhibited high stability via XRD, FT-IR, and DRS tests. Therefore, green ZnO particles synthesized using *Chrysanthemum* spp. flower extract could be an excellent photocatalyst for the degradation of organic dyes in real wastewaters.

Author Contributions: Conceptualization, T.V.T. and C.V.N.; methodology, M.A.; software, F.A.H.; validation, W.N., D.T.D.N. and C.V.N.; formal analysis, M.A.; investigation, T.V.T.; resources, W.N.; data curation, D.T.D.N.; writing—original draft preparation, T.V.T.; writing—review and editing, T.V.T.; visualization, C.V.N.; supervision, C.V.N.; project administration, M.A.; funding acquisition, M.A. All authors have read and agreed to the published version of the manuscript.

Data Availability Statement: The data presented in this study are available on request from the corresponding author. The data are not publicly available due to privacy concerns.

Conflicts of Interest: The authors declare no conflict of interest.

References

1. Hassan, M.M.; Carr, C.M. A critical review on recent advancements of the removal of reactive dyes from dyehouse effluent by ion-exchange adsorbents. *Chemosphere* **2018**, *209*, 201–219. [CrossRef]
2. Donkadokula, N.Y.; Kola, A.K.; Naz, I.; Saroj, D. A review on advanced physico-chemical and biological textile dye wastewater treatment techniques. *Rev. Environ. Sci. Bio/Technol.* **2020**, *19*, 543–560. [CrossRef]
3. Nguyen, L.T.T.; Vo, D.-V.N.; Nguyen, L.T.H.; Duong, A.T.T.; Nguyen, H.Q.; Chu, N.M.; Nguyen, D.T.C.; Tran, T. Van Synthesis, characterization, and application of ZnFe$_2$O$_4$@ZnO nanoparticles for photocatalytic degradation of Rhodamine B under visible-light illumination. *Environ. Technol. Innov.* **2022**, *25*, 102130. [CrossRef]
4. Ahmad, A.; Khan, N.; Giri, B.S.; Chowdhary, P.; Chaturvedi, P. Removal of methylene blue dye using rice husk, cow dung and sludge biochar: Characterization, application, and kinetic studies. *Bioresour. Technol.* **2020**, *306*, 123202. [CrossRef]
5. Din, M.I.; Khalid, R.; Najeeb, J.; Hussain, Z. Fundamentals and photocatalysis of methylene blue dye using various nanocatalytic assemblies- a critical review. *J. Clean. Prod.* **2021**, *298*, 126567. [CrossRef]
6. Dutt, M.A.; Hanif, M.A.; Nadeem, F.; Bhatti, H.N. A review of advances in engineered composite materials popular for wastewater treatment. *J. Environ. Chem. Eng.* **2020**, *8*, 104073. [CrossRef]

7. Zhu, X.; Zhou, Q.; Xia, Y.; Wang, J.; Chen, H.; Xu, Q.; Liu, J.; Feng, W.; Chen, S. Preparation and characterization of Cu-doped TiO$_2$ nanomaterials with anatase/rutile/brookite triphasic structure and their photocatalytic activity. *J. Mater. Sci. Mater. Electron.* **2021**, *32*, 21511–21524. [CrossRef]

8. Ong, C.B.; Ng, L.Y.; Mohammad, A.W. A review of ZnO nanoparticles as solar photocatalysts: Synthesis, mechanisms and applications. *Renew. Sustain. Energy Rev.* **2018**, *81*, 536–551. [CrossRef]

9. Nguyen, N.T.T.; Nguyen, L.M.; Nguyen, T.T.T.; Nguyen, T.T.; Nguyen, D.T.C.; Tran, T. Van Formation, antimicrobial activity, and biomedical performance of plant-based nanoparticles: A review. *Environ. Chem. Lett.* **2022**, *20*, 2531–2571. [CrossRef]

10. Zhu, X.; Wang, J.; Yang, D.; Liu, J.; He, L.; Tang, M.; Feng, W.; Wu, X. Fabrication, characterization and high photocatalytic activity of Ag–ZnO heterojunctions under UV-visible light. *RSC Adv.* **2021**, *11*, 27257–27266. [CrossRef]

11. Ameen, F.; Dawoud, T.; AlNadhari, S. Ecofriendly and low-cost synthesis of ZnO nanoparticles from *Acremonium potronii* for the photocatalytic degradation of azo dyes. *Environ. Res.* **2021**, *202*, 111700. [CrossRef]

12. Zaidi, Z.; Siddiqui, S.I.; Fatima, B.; Chaudhry, S.A. Synthesis of ZnO nanospheres for water treatment through adsorption and photocatalytic degradation: Modelling and process optimization. *Mater. Res. Bull.* **2019**, *120*, 110584. [CrossRef]

13. Chen, X.; Wu, Z.; Liu, D.; Gao, Z. Preparation of ZnO photocatalyst for the efficient and rapid photocatalytic degradation of azo dyes. *Nanoscale Res. Lett.* **2017**, *12*, 143. [CrossRef]

14. Davari, N.; Farhadian, M.; Solaimany Nazar, A.R. Synthesis and characterization of Fe$_2$O$_3$ doped ZnO supported on clinoptilolite for photocatalytic degradation of metronidazole. *Environ. Technol.* **2021**, *42*, 1734–1746. [CrossRef]

15. Basnet, P.; Inakhunbi Chanu, T.; Samanta, D.; Chatterjee, S. A review on bio-synthesized zinc oxide nanoparticles using plant extracts as reductants and stabilizing agents. *J. Photochem. Photobiol. B Biol.* **2018**, *183*, 201–221. [CrossRef]

16. Nguyen, N.T.T.; Nguyen, L.M.; Nguyen, T.T.T.; Liew, R.K.; Nguyen, D.T.C.; Tran, T. Van Recent advances on botanical biosynthesis of nanoparticles for catalytic, water treatment and agricultural applications: A review. *Sci. Total Environ.* **2022**, *827*, 154160. [CrossRef]

17. Gao, Y.; Xu, D.; Ren, D.; Zeng, K.; Wu, X. Green synthesis of zinc oxide nanoparticles using *Citrus sinensis* peel extract and application to strawberry preservation: A comparison study. *LWT* **2020**, *126*, 109297. [CrossRef]

18. Khan, Z.U.H.; Sadiq, H.M.; Shah, N.S.; Khan, A.U.; Muhammad, N.; Hassan, S.U.; Tahir, K.; Khan, F.U.; Imran, M.; Ahmad, N. Greener synthesis of zinc oxide nanoparticles using *Trianthema portulacastrum* extract and evaluation of its photocatalytic and biological applications. *J. Photochem. Photobiol. B Biol.* **2019**, *192*, 147–157. [CrossRef]

19. Darvishi, E.; Kahrizi, D.; Arkan, E. Comparison of different properties of zinc oxide nanoparticles synthesized by the green (using *Juglans regia* L. leaf extract) and chemical methods. *J. Mol. Liq.* **2019**, *286*, 110831. [CrossRef]

20. Nguyen, D.T.C.; Le, H.T.N.; Nguyen, T.T.; Nguyen, T.T.T.; Bach, L.G.; Nguyen, T.D.; Tran, T. Van Multifunctional ZnO nanoparticles bio-fabricated from *Canna indica* L. flowers for seed germination, adsorption, and photocatalytic degradation of organic dyes. *J. Hazard. Mater.* **2021**, *420*, 126586. [CrossRef]

21. Asha, S.; Bessy, T.C.; Joe Sherin, J.F.; Vani, C.V.; Kumar, C.V.; Bindhu, M.R.; Sureshkumar, S.; Al-Khattaf, F.S.; Hatamleh, A.A. Efficient photocatalytic degradation of industrial contaminants by *Piper longum* mediated ZnO nanoparticles. *Environ. Res.* **2022**, *208*, 112686. [CrossRef]

22. Bhattacharjee, N.; Som, I.; Saha, R.; Mondal, S. A critical review on novel eco-friendly green approach to synthesize zinc oxide nanoparticles for photocatalytic degradation of water pollutants. *Int. J. Environ. Anal. Chem.* **2022**, 1–28. [CrossRef]

23. Egbosiuba, T.C.; Abdulkareem, A.S.; Tijani, J.O.; Ani, J.I.; Krikstolaityte, V.; Srinivasan, M.; Veksha, A.; Lisak, G. Taguchi optimization design of diameter-controlled synthesis of multi walled carbon nanotubes for the adsorption of Pb(II) and Ni(II) from chemical industry wastewater. *Chemosphere* **2021**, *266*, 128937. [CrossRef]

24. Moralı, U.; Demiral, H.; Şensöz, S. Optimization of activated carbon production from sunflower seed extracted meal: Taguchi design of experiment approach and analysis of variance. *J. Clean. Prod.* **2018**, *189*, 602–611. [CrossRef]

25. Maazinejad, B.; Mohammadnia, O.; Ali, G.A.M.; Makhlouf, A.S.H.; Nadagouda, M.N.; Sillanpää, M.; Asiri, A.M.; Agarwal, S.; Gupta, V.K.; Sadegh, H. Taguchi L9 (34) orthogonal array study based on methylene blue removal by single-walled carbon nanotubes-amine: Adsorption optimization using the experimental design method, kinetics, equilibrium and thermodynamics. *J. Mol. Liq.* **2020**, *298*, 112001. [CrossRef]

26. Youssef, F.S.; Eid, S.Y.; Alshammari, E.; Ashour, M.L.; Wink, M.; El-Readi, M.Z. *Chrysanthemum indicum* and *Chrysanthemum morifolium*: Chemical Composition of Their Essential Oils and Their Potential Use as Natural Preservatives with Antimicrobial and Antioxidant Activities. *Foods* **2020**, *9*, 1460. [CrossRef]

27. Naseer, M.; Aslam, U.; Khalid, B.; Chen, B. Green route to synthesize Zinc Oxide Nanoparticles using leaf extracts *of Cassia fistula* and *Melia azadarach* and their antibacterial potential. *Sci. Rep.* **2020**, *10*, 9055. [CrossRef]

28. Nilavukkarasi, M.; Vijayakumar, S.; Prathipkumar, S. *Capparis zeylanica* mediated bio-synthesized ZnO nanoparticles as antimicrobial, photocatalytic and anti-cancer applications. *Mater. Sci. Energy Technol.* **2020**, *3*, 335–343. [CrossRef]

29. Dhiman, P.; Sharma, S.; Kumar, A.; Shekh, M.; Sharma, G.; Naushad, M. Rapid visible and solar photocatalytic Cr(VI) reduction and electrochemical sensing of dopamine using solution combustion synthesized ZnO–Fe$_2$O$_3$ nano heterojunctions: Mechanism Elucidation. *Ceram. Int.* **2020**, *46*, 12255–12268. [CrossRef]

30. Golmohammadi, M.; Honarmand, M.; Ghanbari, S. A green approach to synthesis of ZnO nanoparticles using jujube fruit extract and their application in photocatalytic degradation of organic dyes. *Spectrochim. Acta Part A Mol. Biomol. Spectrosc.* **2020**, *229*, 117961. [CrossRef]

31. Nithya, K.; Kalyanasundharam, S. Effect of chemically synthesis compared to biosynthesized ZnO nanoparticles using aqueous extract of C. halicacabum and their antibacterial activity. *OpenNano* **2019**, *4*, 100024. [CrossRef]

32. Alyamani, A.A.; Albukhaty, S.; Aloufi, S.; AlMalki, F.A.; Al-Karagoly, H.; Sulaiman, G.M. Green Fabrication of Zinc Oxide Nanoparticles Using Phlomis Leaf Extract: Characterization and In Vitro Evaluation of Cytotoxicity and Antibacterial Properties. *Molecules* **2021**, *26*, 6140. [CrossRef]

33. Pugazhendhi, A.; Prabhu, R.; Muruganantham, K.; Shanmuganathan, R.; Natarajan, S. Anticancer, antimicrobial and photo-catalytic activities of green synthesized magnesium oxide nanoparticles (MgONPs) using aqueous extract of *Sargassum wightii*. *J. Photochem. Photobiol. B Biol.* **2019**, *190*, 86–97. [CrossRef]

34. Dobrucka, R. Synthesis of MgO Nanoparticles Using *Artemisia abrotanum* Herba Extract and Their Antioxidant and Photocatalytic Properties. *Iran. J. Sci. Technol. Trans. A Sci.* **2018**, *42*, 547–555. [CrossRef]

35. Essien, E.R.; Atasie, V.N.; Oyebanji, T.O.; Nwude, D.O. Biomimetic synthesis of magnesium oxide nanoparticles using *Chromolaena odorata* (L.) leaf extract. *Chem. Pap.* **2020**, *74*, 2101–2109. [CrossRef]

36. Abdallah, Y.; Ogunyemi, S.O.; Abdelazez, A.; Zhang, M.; Hong, X.; Ibrahim, E.; Hossain, A.; Fouad, H.; Li, B.; Chen, J. The green synthesis of MgO nano-Flowers using *Rosmarinus officinalis* L. (Rosemary) and the antibacterial activities against *Xanthomonas oryzae* pv. *oryzae*. *BioMed Res. Int.* **2019**, *2019*, 5620989. [CrossRef]

37. Faisal, S.; Jan, H.; Shah, S.A.; Shah, S.; Khan, A.; Akbar, M.T.; Rizwan, M.; Jan, F.; Wajidullah; Akhtar, N.; et al. Green Synthesis of Zinc Oxide (ZnO) Nanoparticles Using Aqueous Fruit Extracts of *Myristica fragrans*: Their Characterizations and Biological and Environmental Applications. *ACS Omega* **2021**, *6*, 9709–9722. [CrossRef]

38. Jeevanandam, J.; Chan, Y.S.; Danquah, M.K. Biosynthesis and characterization of MgO nanoparticles from plant extracts via induced molecular nucleation. *New J. Chem.* **2017**, *41*, 2800–2814. [CrossRef]

39. Ramesh, M.; Anbuvannan, M.; Viruthagiri, G. Green synthesis of ZnO nanoparticles using *Solanum nigrum* leaf extract and their antibacterial activity. *Spectrochim. Acta Part A Mol. Biomol. Spectrosc.* **2015**, *136*, 864–870. [CrossRef]

40. Chinnasamy, C.; Tamilselvam, P.; Karthick, B.; Sidharth, B.; Senthilnathan, M. Green Synthesis, Characterization and Optimization Studies of Zinc Oxide Nano Particles Using Costusigneus Leaf Extract. *Mater. Today Proc.* **2018**, *5*, 6728–6735. [CrossRef]

41. Handani, S.; Emriadi; Dahlan, D.; Arief, S. Enhanced structural, optical and morphological properties of ZnO thin film using green chemical approach. *Vacuum* **2020**, *179*, 109513. [CrossRef]

42. Thi, T.U.D.; Nguyen, T.T.; Thi, Y.D.; Thi, K.H.T.; Phan, B.T.; Pham, K.N. Green synthesis of ZnO nanoparticles using orange fruit peel extract for antibacterial activities. *RSC Adv.* **2020**, *10*, 23899–23907.

43. Soto-Robles, C.A.; Luque, P.A.; Gómez-Gutiérrez, C.M.; Nava, O.; Vilchis-Nestor, A.R.; Lugo-Medina, E.; Ranjithkumar, R.; Castro-Beltrán, A. Study on the effect of the concentration of *Hibiscus sabdariffa* extract on the green synthesis of ZnO nanoparticles. *Results Phys.* **2019**, *15*, 102807. [CrossRef]

44. Thakur, S.; Shandilya, M.; Guleria, G. Appraisement of antimicrobial zinc oxide nanoparticles through Cannabis *Jatropha curcasa* Alovera and Tinosporacordifolia leaves by green synthesis process. *J. Environ. Chem. Eng.* **2021**, *9*, 104882. [CrossRef]

45. Şahin, B.; Soylu, S.; Kara, M.; Türkmen, M.; Aydin, R.; Çetin, H. Superior antibacterial activity against seed-borne plant bacterial disease agents and enhanced physical properties of novel green synthesized nanostructured ZnO using *Thymbra spicata* plant extract. *Ceram. Int.* **2021**, *47*, 341–350. [CrossRef]

46. Zhu, W.; Hu, C.; Ren, Y.; Lu, Y.; Song, Y.; Ji, Y.; Han, C.; He, J. Green synthesis of zinc oxide nanoparticles using *Cinnamomum camphora* (L.) Presl leaf extracts and its antifungal activity. *J. Environ. Chem. Eng.* **2021**, *9*, 106659. [CrossRef]

47. Chauhan, A.K.; Kataria, N.; Garg, V.K. Green fabrication of ZnO nanoparticles using Eucalyptus spp. leaves extract and their application in wastewater remediation. *Chemosphere* **2020**, *247*, 125803. [CrossRef]

48. Alshehri, A.A.; Malik, M.A. Biogenic fabrication of ZnO nanoparticles using *Trigonella foenum-graecum* (Fenugreek) for proficient photocatalytic degradation of methylene blue under UV irradiation. *J. Mater. Sci. Mater. Electron.* **2019**, *30*, 16156–16173. [CrossRef]

49. Kumar, M.A.P.; Suresh, D.; Nagabhushana, H.; Sharma, S.C. *Beta vulgaris* aided green synthesis of ZnO nanoparticles and their luminescence, photocatalytic and antioxidant properties. *Eur. Phys. J. Plus* **2015**, *130*, 1–7.

50. Madhumitha, G.; Fowsiya, J.; Gupta, N.; Kumar, A.; Singh, M. Green synthesis, characterization and antifungal and photocatalytic activity of *Pithecellobium dulce* peel–mediated ZnO nanoparticles. *J. Phys. Chem. Solids* **2019**, *127*, 43–51. [CrossRef]

51. Shim, Y.J.; Soshnikova, V.; Anandapadmanaban, G.; Mathiyalagan, R.; Jimenez Perez, Z.E.; Markus, J.; Ju Kim, Y.; Castro-Aceituno, V.; Yang, D.C. Zinc oxide nanoparticles synthesized by *Suaeda japonica* Makino and their photocatalytic degradation of methylene blue. *Optik* **2019**, *182*, 1015–1020. [CrossRef]

52. Soto-Robles, C.A.; Nava, O.; Cornejo, L.; Lugo-Medina, E.; Vilchis-Nestor, A.R.; Castro-Beltrán, A.; Luque, P.A. Biosynthesis, characterization and photocatalytic activity of ZnO nanoparticles using extracts of *Justicia spicigera* for the degradation of methylene blue. *J. Mol. Struct.* **2021**, *1225*, 129101. [CrossRef]

53. Sun, L.; Shao, Q.; Zhang, Y.; Jiang, H.; Ge, S.; Lou, S.; Lin, J.; Zhang, J.; Wu, S.; Dong, M. N self-doped ZnO derived from microwave hydrothermal synthesized zeolitic imidazolate framework-8 toward enhanced photocatalytic degradation of methylene blue. *J. Colloid Interface Sci.* **2020**, *565*, 142–155. [CrossRef]

54. Chen, L.; Batjikh, I.; Hurh, J.; Han, Y.; Huo, Y.; Ali, H.; Li, J.F.; Rupa, E.J.; Ahn, J.C.; Mathiyalagan, R.; et al. Green synthesis of zinc oxide nanoparticles from root extract of *Scutellaria baicalensis* and its photocatalytic degradation activity using methylene blue. *Optik* **2019**, *184*, 324–329. [CrossRef]
55. Mardikar, S.P.; Kulkarni, S.; Adhyapak, P. V Sunlight driven highly efficient degradation of methylene blue by CuO-ZnO nanoflowers. *J. Environ. Chem. Eng.* **2020**, *8*, 102788. [CrossRef]